Trends of Water Gas Shift Reaction on Close-Packed Transition Metal Surfaces

ARTICLE *in* THE JOURNAL OF PHYSICAL CHEMISTRY C · MAY 2010

Impact Factor: 4.77 · DOI: 10.1021/jp1005814

3 AUTHORS, INCLUDING:

Jeng-Han Wang
National Taiwan Normal University
46 PUBLICATIONS **979** CITATIONS

SEE PROFILE

Trends of Water Gas Shift Reaction on Close-Packed Transition Metal Surfaces

Shih-Chang Huang, Chia-Hao Lin, and J.-H. Wang*

Department of Chemistry, National Taiwan Normal University, Taipei, Taiwan

Received: January 20, 2010; Revised Manuscript Received: April 1, 2010

The mechanism of the water gas shift reaction (WGSR) on the close-packed transition metal surfaces of Co, Ni, Cu (from the 3d row), Rh, Pd, Ag (from the 4d row), Ir, Pt, and Au (from the 5d row) has been systematically examined by periodic density functional theory (DFT) calculations. The comparison of potential energy surface (PES) concludes that WGSR activity is influenced by two kinds of elementary steps: O−H bond dissociation and C−O bond formation. Activation barriers (Ea) and reaction energies (ΔH) on a series of metal surfaces show good BEP relationship; however, their energetic trends are opposite in these two kinds of steps. In O−H bond dissociation steps, trends of Ea and ΔH are groups 9 < 10 < 11 and 3d < 4d < 5d. On the other hand, C−O bond formation steps on the surfaces of the lower-right metals in the d block (Cu, Ag, Pt, Au) have relatively lower Ea and ΔH, which is responsible for their high WGSR activity of metal/oxide catalysts. In addition, the fundamental of energetic trends has been examined from the analyses of adsorption energy, density of state (DOS), and charge density. The result shows that the surfaces of upper-left d-block metals (Co, Ni, Rh) with higher energy and smaller delocalization of their d orbitals yield a stronger adsorption energy with higher induced charges that will stabilize dissociating fragments to lower the barrier and retard desorptions to lift the barrier in O−H bond dissociation and C−O bond formation steps, respectively. The prediction of energetic trends in the present work is also appropriate for other catalytic reactions, such as ethanol decomposition and CO oxidation, and can help us scientifically design a better catalyst for the desired reaction.

Introduction

The water gas shift reaction (WGSR), $CO + H_2O \rightarrow CO_2 + H_2 \rightarrow H_{298} = -41.2$ kJ/mol, is well established and widely applied in the chemical industry for H_2 production.[1] The moderate exothermic WGSR requires low temperatures to achieve low CO concentration. On the other hand, the favorable kinetics is at a higher temperature. As a result, WGSR is typically carried out in two steps: a high-temperature operation at 350−500 °C with iron/oxide-based catalyst to rapidly convert CO and a low-temperature operation at 180−250 °C with copper/oxide-based catalysts to achieve lower equilibrium CO content.[2,3] Recently, WGSR has sparked renewed interest due to its application in the rapid innovation in fuel cell technology and plays a key role in the steam reforming of hydrocarbon and biomass fuels. The importance of WGSR is that it removes the poisonous CO, which is a side product in the production of hydrogen fuel, and produces extra H_2 fuel.

Numerous experimental and computational efforts have been conducted to find more efficient catalysts and elucidate the mechanism. Experimentally, the WGSR activity of catalysts with Fe, Co, Ni, Cu, Ru, Rh, Pd, Ag, Re, Os, Ir, Pt, and Au supported on the metal oxides of TiO_2, ZnO, CeO_2, La_2O_3, ZrO_2, Al_2O_3, MgO, Fe_2O_3, Cr_2O_3, and SiO_2 has been extensively studied.[4−17] The result concludes that, except group 11 elements, Pt has better performances than other transition metals, and the catalytic activity of pure metals is a few orders of magnitude as they are supported on the oxides of TiO_2 and CeO_2. Furthermore, the WGSR mechanism on the promising catalysts, (Cu, Ag, Pt, Au)/(TiO_2, CeO_2), has been widely studied by various *in situ* techniques, including scanning tunneling microscopy (STM),[18−24] temperature-programmed reduction (TPR),[23,25−27] time-resolved X-ray diffraction (XRD),[25,28,29] X-ray absorption near edge spectroscopy (XANES),[7,8,29,30] and diffuse reflectance infrared Fourier transform spectroscopy (DRIFTS),[8,23,27,30,31] and common *ex situ* characterization methods, including X-ray photoelectron spectroscopy (XPS), Auger electron spectroscopy (AES), ultraviolet photoelectron spectroscopy (UPS), and transmission electron microscopy (TEM).[2,8,18,20−24,26,28−34] These studies show that both metals and oxides have significant influence on the catalytic activity. Metals are positively charged through WGSR and back to their metallic property after the reaction. Oxides help for water dissociation steps, and their oxygen vacancy plays a key role in the reaction. The significance of oxides has recently been proven from the inverse catalyst with oxide/metal forms as well.[21,22,35]

Computationally, the WGSR mechanism on the pure metal surfaces of Cu,[32,36,37] Pt,[38] and Au[32,37,39−41] and metal/oxide catalysts of Au/CeO_2,[42] (Au, Cu)/TiO_2,[20] Pt/CeO_2,[43] and (TiO_x, CeO_x)/(Cu, Au)[21,22,24] has been widely elucidated by first-principles calculations. The computed result shows that the mechanism corresponds to the oxidation of CO by water dissociated OH or O forming the key intermediate of carbonyl. The other intermediate of formate, which is observed from the experiment, is considered as a spectator species.[36] The rate-determining step of WGSR is in the initial water dissociation on pure metal surfaces. The related high dissociation barrier of this step can be reduced more than a half, while water is dissociating on oxide surfaces or by a hydrogen abstracting process. Despite numerous experimental and computational efforts, most of the studies in the mechanism investigation only focus on a single catalyst, and no trends have been concluded. Without systematic comparison on a series of catalysts, the mechanism remains uncertain, and the advantages of coinage-

* Corresponding author. Tel.: (+886)2-7734-6123. Fax: (+886)2-2932-4249. E-mail: jenghan@ntnu.edu.tw.

10.1021/jp1005814
Published on Web 05/07/2010

TABLE 1: Adsorption Energies (eV) of Reactants, Intermediates, and Products on the Close-Packed Metal Surfaces

	Co	Ni	Cu	Rh	Pd	Ag	Ir	Pt	Au
$CO_{(a)}$	−1.80	−1.99	−0.91	−1.99	−2.01	−0.17	−1.74	−1.87	−0.38
$H_2O_{(a)}$	−0.35	−0.33	−0.26	−0.37	−0.30	−0.19	−0.39	−0.29	−0.12
$OH_{(a)}$	−3.64	−3.42	−3.32	−3.10	−2.62	−2.79	−2.71	−2.34	−2.21
$O_{(a)}$	−5.93	−5.68	−5.13	−5.40	−4.58	−3.90	−5.17	−4.53	−3.56
$H_{(a)}$	−2.78	−2.76	−2.51	−2.86	−2.87	−2.09	−2.76	−2.78	−2.20
cis-$COOH_{(a)}$	−2.30	−2.36	−1.92	−2.50	−2.38	−1.60	−2.37	−2.42	−1.72
$CO_{2(a)}$	0.01	−0.02	−0.02	0.00	−0.01	−0.01	0.01	0.00	−0.02

metal- and Pt-based catalysts in WGSR still cannot be rationally understood from previous works.

In this study, we employ periodic density functional theory (DFT) calculations to examine the WGSR mechanism on 3d to 5d metal surfaces of groups 9 (Co, Rh, and Ir), 10 (Ni, Pd, and Pt), and 11 (Cu, Ag, and Au) with the same crystal structure and surface orientation. The activation barriers (Ea) and reaction energies (ΔH) of the complete potential energy surface (PES) have been systematically computed and compared. In addition, energetic trends on the selected metal surfaces have been extensively discussed and further applied to justify the catalytic activity.

Methods

The Vienna ab initio Simulation Package (VASP),[44−46] implementing the DFT with a 3D periodic boundary condition, has been employed for calculations. The exchange-correlation function is treated by the generalized gradient approximation[47] with Perdew−Wang 1991 formulation (GGA-PW91).[48] The electron−ion interaction is modeled by the projector-augmented wave method (PAW),[49,50] combining the accuracy of augmented plane waves with the cost-effective pseudopotentials. The basis of plane waves has a kinetic cutoff energy at 600 eV. The Brillouin-Zone (BZ) integration is sampled at the 0.05 × 2 (1/Å) interval in the reciprocal space by a Monkhorst−Pack scheme.[51]

The most stable (111) surface of the close-packed crystals is modeled by a five-layer metal slab with a 4 × 4 surface unit cell to limit the artificial interaction from adsorbates in repeating super cells. An equivalent five-layer vacuum space is applied to minimize the interaction between distinct slabs. The bottom two layers of the modeled slab are fixed at the computed lattice constants to represent the semi-infinite bulk crystal (beneath the surface), and the top three layers are free to relax in the calculations of surface adsorption and interfacial reaction. The spin-polarized calculation is included in the case of ferromagnetic Co(111) and Ni(111). The convergence (up to 0.05 eV) with respect to the k-point, cutoff energy, as well as number of metal layers is confirmed.

The Nudged Elastic Band (NEB) method,[52] applied by simultaneously relaxing an interpolated chain of configurations between the initial and final positions along the minimum energy pathway (MEP), is employed to locate transition states for all elementary steps. The computed Ea values are also correlated with ΔH in the Brønsted−Evans−Polanyi (BEP) relation.

Results

The preferential WGSR, involving the oxidation of CO by H_2O and its fragments, might lead into three possible routes as CO initially reacts with H_2O (no dissociation), OH (after one H dissociation), and O (after two successive H dissociation) in reactions 1, 2, and 3, respectively.

$$CO_{(a)} + H_2O_{(a)} \rightarrow COOH_{2(a)} \text{ (not possible)} \quad (1)$$

$$CO_{(a)} + H_2O_{(a)} \rightarrow CO_{(a)} + OH_{(a)} + H_{(a)} \rightarrow COOH_{(a)} + H_{(a)} \rightarrow CO_{2(a)} + 2H_{(a)} \rightarrow CO_{2(g)} + H_{2(g)} \quad (2)$$

$$CO_{(a)} + H_2O_{(a)} \rightarrow CO_{(a)} + OH_{(a)} + H_{(a)} \rightarrow CO_{(a)} + O_{(a)} + 2H_{(a)} \rightarrow CO_{2(a)} + 2H_{(a)} \rightarrow CO_{2(g)} + H_{2(g)} \quad (3)$$

After an extensive search, we conclude that $CO_{(a)}$ cannot directly react with stable $H_2O_{(a)}$, and reaction 1 is not possible. In reaction 2, $CO_{(a)}$ is oxidized by $OH_{(a)}$, forming a $COOH_{(a)}$ intermediate, and ultimately yields the products of $CO_{2(g)}$ and $H_{2(g)}$. The $COOH_{(a)}$ intermediate is more likely to form carboxyl adsorption than bidentate formate since $CO_{(a)}$ is bonded with metal surfaces through its C atom.[36] Reaction 2 is known as a carboxyl mechanism and is considered as the most feasible reaction route in the previous works on Cu(111), Cu_{29} nanoparticle, Pt(111), Pt/CeO_2, Au(111), Au/CeO_2, and Au_{29} nanoparticle.[32,36,38,41,42,53,54]

In reaction 3, $CO_{(a)}$ is oxidized by atomic $O_{(a)}$ and forms $CO_{2(a)}$ after two consecutive O−H bond dissociations of $H_2O_{(a)}$. In previous studies,[55−62] $CO_{(a)} + O_{(a)} + 2H_{(a)} \rightarrow CO_{2(a)} + 2H_{(a)}$ is considered as the important step of the CO oxidation process, while $H_{(a)}$ plays as a spectator. Therefore, both reactions 2 and 3 on the nine selected metal surfaces are taken into account in the present work.

Adsorption. The adsorption of the reactants ($CO_{(a)}$ and $H_2O_{(a)}$), product ($CO_{2(a)}$), and intermediates ($OH_{(a)}$, $O_{(a)}$, $H_{(a)}$, and $COOH_{(a)}$) in reactions 2 and 3 is initially optimized for the mechanism study. The adsorption energies of the adspecies are listed in Table 1. Since the adsorption structures are similar on close-packed metal surfaces, only the optimized structures on Rh(111) are shown in Figure 1 for brevity.

The reactant of $CO_{(a)}$ has a stable adsorption on the FCC site through its C atom, while $H_2O_{(a)}$ is preferentially adsorbing on the top site (Figure 1). The computed adsorption energies of $CO_{(a)}$ and $H_2O_{(a)}$ are in the ranges of −0.17 to −2.01 and −0.12 to −0.39 eV, respectively (Table 1). The product of $CO_{2(a)}$ is a stable molecule and has negligible adsorption energy on all surfaces, i.e., $CO_{2(a)} = CO_{2(g)}$. The intermediates of $OH_{(a)}$, $O_{(a)}$, and $H_{(a)}$ all have the preference of FCC-site adsorption with the adsorption energies in ranges of −2.21 to −3.64, −3.56 to −5.93, and −2.09 to −2.87 eV, respectively. The other intermediate of $COOH_{(a)}$ prefers to adsorb on the top site and has two stable *cis* and *trans* forms as the O−H bond points away and toward the surface, respectively. Since $COOH_{(a)}$ is formed through $CO_{(a)} + OH_{(a)} \rightarrow COOH_{(a)}$ in reaction 2 while $OH_{(a)}$ bonds to the surface through its O atom, *cis*-$COOH_{(a)}$ is the likely intermediate in WGSR.[36,38] The adsorption energy of *cis*-$COOH_{(a)}$ is in the range of −1.60 to −2.50 eV in the present calculation.

The computed adsorption energies show good agreement with previous works for $CO_{(a)}$,[36,38,39,62−68] $H_2O_{(a)}$,[36,38,39,64,69−71]

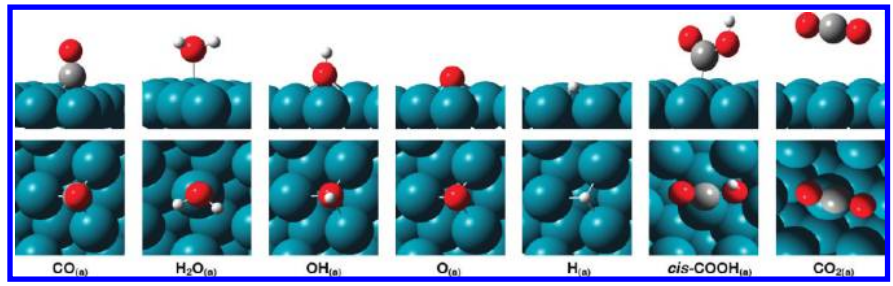

Figure 1. Side and top views of $CO_{(a)}$, $H_2O_{(a)}$, $OH_{(a)}$, $O_{(a)}$, $H_{(a)}$, $COOH_{(a)}$, and $CO_{2(a)}$ on Rh(111). The relative adsorption energies are listed in Table 1. Gray, red, white, and cyan spheres mark C, O, H, and Rh atoms, respectively.

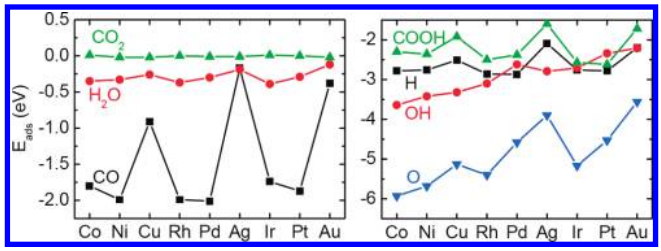

Figure 2. Comparison of adsorption energies of reactants, product (left), and intermediates (right) on the close-packed metal surfaces. The energetic parameters are listed in Table 1.

$CO_{2(a)}$,[36,38,39,41,64] $OH_{(a)}$,[36,38,64,69,72] $O_{(a)}$,[66,67,71−75] $H_{(a)}$,[36,38,64,66,71,76] and *cis*-$COOH_{(a)}$[36,38,41] as summarized in Table S1 (Supporting Information). Our calculation might show stronger adsorption energies than previous works in some cases. This difference can be attributed to our larger (4 × 4) surface model, which can distribute the bonding electron efficiently and increase the bond strength.

Comparing different adsorptions on the same metal surface, intermediates have relatively stronger adsorption energies than both reactants and products. As compared in Figure 2, the adsorption energies of $CO_{(a)}$, $H_2O_{(a)}$, and $CO_{2(a)}$ are smaller than 2.00 eV, while those of $OH_{(a)}$, $O_{(a)}$, $H_{(a)}$, and *cis*-$COOH_{(a)}$ are mostly larger than 2.00 eV. The stronger adsorption energies of intermediates correspond to the higher activity of OH, O, H, and COOH radicals in the gas phase.

Comparing the identical adsorption on different metal surfaces, the adsorption energy decreases as the adsorbed surface moves from left to right and from up to down across the Periodic Table (the zigzag lines in Figure 2). For example, Au(111) and Ag(111) have the lowest adsorption energies, whereas Co(111) and Ni(111) have the highest ones in most of the adsorptions. This trend, which purely corresponds to electronic structures of metal surfaces, can be utilized to understand the mechanism of WGSR and will be described thoroughly in the Discussion.

Mechanism. The MEP of each elementary step in reactions 2 and 3 is examined by computing each transition state between two local minima. By integrating these MEPs, the complete PES can be obtained for the mechanism study. The PES of WGSR and related geometrical structures on the Rh(111) surface, for example, are shown in Figures 3 and 4, respectively. The corresponding Ea and ΔH on the metal surfaces are listed in Table 2 and compared in Figure 5. Their correlations are summarized in the BEP diagrams in Figure 6.

The first step of WGSR is water dissociation: top-adsorbed $H_2O_{(a)}$ dissociates to FCC-adsorbed $H_{(a)}$ and $OH_{(a)}$, with the activation barrier of Ea_1 and reaction energy of ΔH_1. The reaction is exothermic ($\Delta H_1 < 0$) only on Co(111) and Ni(111) and becomes more endothermic as metal surfaces shift from left to right and up to down across the Periodic Table (black squares in Figure 5). The activation barriers of Ea_1 range from 0.45 to 2.04 eV and show good BEP relationship with ΔH_1, −0.37 to 1.43 eV, as shown in Figure 6.

The dissociated $OH_{(a)}$ can react with coadsorbed $CO_{(a)}$, through the carboxyl mechanism, forming *cis*-$COOH_{(a)}$ on the top site, $CO_{(a)} + OH_{(a)} + H_{(a)} \rightarrow$ *cis*-$COOH_{(a)} + H_{(a)}$. The computed activation barriers of Ea_2 and reaction energies of ΔH_2 are in the ranges of 0.30 to 1.56 and −0.95 to 1.39 eV, respectively. Both ΔH_2 and Ea_2 in this step have a good BEP relationship with the correlation coefficient of $R^2 = 0.97$ and have the same trend that energies decrease as surfaces move from right to left and down to up across the Periodic Table, as shown in red circles in Figure 5. This trend is opposite to that of Ea_1 and ΔH_1 in the O−H bond breaking step.

The intermediate of *cis*-$COOH_{(a)}$ can further dissociate its H forming $CO_{2(a)}$ with two atomic $H_{(a)}$ adsorbed on neighboring FCC sites, *cis*-$COOH_{(a)} + H_{(a)} \rightarrow CO_{2(a)} + 2H_{(a)}$. The computed activation barriers (Ea_3) and reaction energies (ΔH_3) are the smallest among all steps on most of metal surfaces (green triangles in Figure 5). In the small ranges of Ea_3 and ΔH_3, 0.55 to 0.61 and −0.59 to −0.49 eV, respectively, no significant trend of them can be concluded, and their BEP correlation is rather poor with the coefficient of $R^2 \sim 0$.

An alternative reaction route (the red dashed line in Figure 2) starts with the second O−H bond dissociation step, $CO_{(a)} + OH_{(a)} + H_{(a)} \rightarrow CO_{(a)} + O_{(a)} + 2H_{(a)}$. The products of atomic $H_{(a)}$ and $O_{(a)}$ adsorb on neighboring FCC sites (Figure 4). The computed activation barriers of Ea_4 (0.76 to 2.31 eV) and reaction energies of ΔH_4 (−0.18 to 1.73 eV) in this step (blue open squares in Figure 5) are comparable to Ea_1 and ΔH_1, respectively, in the first O−H bond dissociation step and have good BEP correlation ($R^2 = 0.96$).

After two consecutive O−H dissociations, atomically adsorbed $O_{(a)}$ will oxidize coadsorbed $CO_{(a)}$ forming $CO_{2(a)}$ through $CO_{(a)} + O_{(a)} + 2H_{(a)} \rightarrow CO_{2(a)} + 2H_{(a)}$. The trend of activation barriers of Ea_5 and reaction energies of ΔH_5 (cyan open circles in Figure 5) is analogous to that of Ea_2 and ΔH_2 in the other C−O bond formation step. In addition, the computed ΔH_5 is in the range of −2.93 to 0.89 eV, which is slightly lower than that of ΔH_2. On the other hand, the range of Ea_5, 0.08 to 1.45 eV, is similar to that of Ea_2. The BEP relationship of Ea_5 and ΔH_5 is also good with a coefficient of $R^2 = 0.98$.

The last step of $CO_{2(a)} + 2H_{(a)} \rightarrow CO_{2(g)} + H_{2(g)}$ corresponds to the desorption of atomically adsorbed $H_{(a)}$ forming $H_{2(g)}$ since $CO_{2(a)}$ has negligible adsorption energy on metal surfaces (Table 1). The computed activation barriers (Ea_6) and reaction energies (ΔH_6) are in ranges of 0.31 to 1.19 and −0.37 to 1.16 eV, respectively, and have a good BEP correlation, $R^2 = 0.98$. The energies decrease as metal surfaces move from left to right and up to down across the Periodic Table (purple diamonds in Figure 5), which is opposite to the trend of $H_{(a)}$ adsorption energies (Figure 2). In addition, the exothermicity of ΔH_6 on Ag(111) and Au(111) implies that $H_{(a)}$ adsorption energies on these

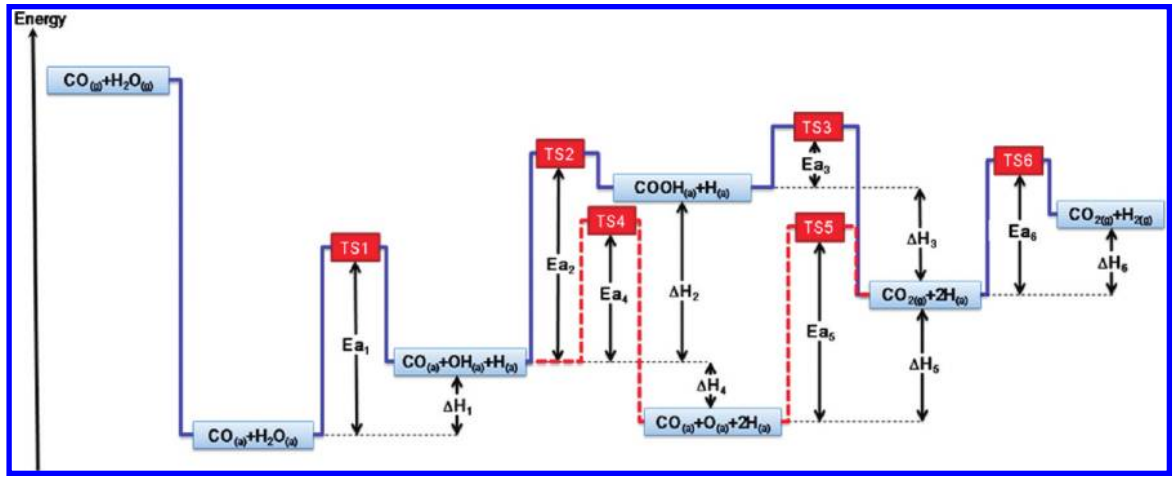

Figure 3. PES of WGSR. The blue (solid) and red (dash) lines are represented as reactions 2 and 3, respectively. The related structures of local minima and transition states on Rh(111) are shown in Figure 4. Ea and ΔH on the close-packed metal surfaces are listed in Table 2.

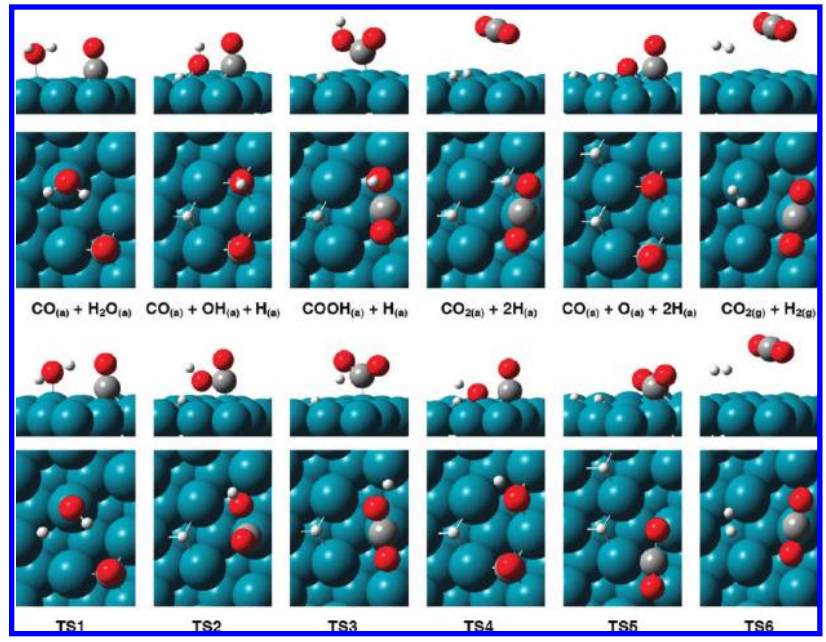

Figure 4. Optimized structures of local minima and transition states of the PES in Figure 3 on Rh(111). Gray, red, white, and cyan spheres mark C, O, H, and Rh atoms, respectively. Top and bottom panels for each pair of images represent side and top views.

TABLE 2: Computed Ea and ΔH (eV) of the PES in Figure 3 on the Close-Packed Metal Surfaces

	Co	Ni	Cu	Rh	Pd	Ag	Ir	Pt	Au
Ea_1	0.45	0.79	1.13	1.00	1.24	1.62	0.80	1.02	2.04
ΔH_1	−0.37	−0.11	0.21	0.16	0.65	0.93	0.18	0.53	1.43
Ea_2	1.56	1.45	0.88	1.06	0.97	0.43	0.79	0.59	0.30
ΔH_2	1.39	1.22	0.44	0.84	0.37	−0.40	0.17	−0.25	−0.95
Ea_3	0.55	0.60	0.60	0.58	0.55	0.61	0.59	0.56	0.58
ΔH_3	−0.56	−0.52	−0.59	−0.56	−0.52	−0.56	−0.56	−0.59	−0.49
Ea_4	0.98	1.09	1.74	0.81	1.35	2.31	0.76	0.95	2.12
ΔH_4	−0.07	−0.03	0.75	−0.09	0.36	1.73	−0.18	0.14	1.49
Ea_5	1.45	1.40	0.62	1.34	0.80	0.09	1.14	0.74	0.08
ΔH_5	0.89	0.73	−0.90	0.57	−0.51	−2.69	0.19	−0.59	−2.93
Ea_6	1.19	1.18	0.66	1.16	1.15	0.31	0.98	1.03	0.45
ΔH_6	1.16	1.15	0.43	1.14	1.15	−0.37	0.93	0.99	−0.18

surfaces are weaker than H−H bonding energy. On the other hand, closed values between Ea_6 and ΔH_6 indicate that the reaction has late transition states on Co(111), Ni(111), Rh(111), Pd(111), Ir(111), and Pt(111).

The computed results show good agreement with previous works. Comparing with previous WGSR calculations on Cu(111)[36] and Pt(111),[38] our computational result shows good agreement with their works in a similar trend, as shown in Table S2 (Supporting Information). The lower Ea_3 and ΔH_3 in the present work can be attributed to the difference between *cis*- and *trans*-$COOH_{(a)}$ employed in the present and previous calculations, respectively. Furthermore, comparing the H_2O dissociation steps in WGSR ($CO_{(a)} + H_2O_{(a)} \rightarrow CO_{(a)} + OH_{(a)} + H_{(a)} \rightarrow CO_{(a)} + O_{(a)} + H_{(a)}$) and in pure water ($H_2O_{(a)} \rightarrow OH_{(a)} + H_{(a)} \rightarrow O_{(a)} +$

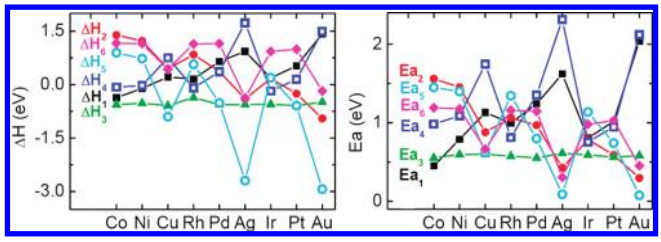

Figure 5. Comparison of ΔH (left) and Ea (right) on the close-packed metal surfaces. The energetic parameters are listed in Table 2.

$2H_{(a)}$),[64,69,70,72,77−80] the computed Ea_1, ΔH_1, Ea_4, and ΔH_4 in the present work (WGSR) have trends and energies similar to those in previous works (pure water dissociation), as listed in Table S3 (Supporting Information). Likewise, the C−O bond formations steps in WGSR ($CO_{(a)} + O_{(a)} + 2H_{(a)} \rightarrow CO_{2(a)} + 2H_{(a)}$) and in pure $CO_{(a)}$ oxidation ($CO_{(a)} + O_{(a)} \rightarrow CO_{2(a)}$).[39,41,57,62,64,80,81] are also comparable and have the same trend (Table S4, Supporting Information). These comparisons imply that the coadsorbed $CO_{(a)}$ or $H_{(a)}$ has limited adsorbate effects in these elementary steps.

In the experiment of pure metal catalysts, Cu is considered as the best one among other transition metals.[32,82] The performance of WGSR on pure metals corresponds to the Ea in the two key steps, O−H bond dissociation and C−O bond formation, which show opposite trends on the metal surfaces. Therefore, except the cheaper price, the top choice of Cu catalyst can be related to the moderate barriers on Cu(111), which locate in the middle of the two opposite trends. In addition, in the experiments of metal/oxide catalysts, (Cu, Ag, Pt, Au)/(TiO_2, CeO_2) show the best performance, as described in the Introduction. The WGSR activity on this kind of catalysts will only correspond to the C−O bond formation barriers, while the O−H bond is breaking on oxide supporters.[21,22] The barriers of O−H bond dissociation on the oxide surfaces of CeO_2 and TiO_2 are found to be smaller, <0.35 eV,[20,43,83,84] than those on all the metal surfaces in the present calculation. Therefore, the excellent activity of (Cu, Ag, Pt, Au)/(TiO_2, CeO_2) can be attributed to the trends of C−O bond formation that lower barriers and occurs on the surfaces of lower-right elements in the Periodic Table: Cu (0.62−0.88 eV), Ag (0.09−0.43 eV), Pt (0.59−0.74 eV), and Au (0.08−0.30 eV).

Discussion

The computed trends of ΔH and Ea in O−H bond dissociation and C−O bond formation steps on the close-packed metal surfaces show good agreement with previous calculations and well clarify the experimental observations. Furthermore, the chemical behavior of the trends can be comprehensively understood from the aspects of adsorption energy, density of state (DOS), and charge density.

Adsorption Energy. The first O−H bond dissociation step of $CO_{(a)} + H_2O_{(a)} \rightarrow CO_{(a)} + OH_{(a)} + H_{(a)}$ can be considered as the combination of the following steps: reactant desorptions ($CO_{(a)} \rightarrow CO_{(g)}$ and $H_2O_{(a)} \rightarrow H_2O_{(g)}$), intermediate dissociation in the gas phase ($H_2O_{(g)} \rightarrow OH_{(g)} + H_{(g)}$), and product adsorptions ($CO_{(g)} \rightarrow CO_{(a)}$, $OH_{(g)} \rightarrow OH_{(a)}$, and $H_{(g)} \rightarrow H_{(a)}$). Therefore, ΔH_1 can be exactly expressed as

$$\Delta H_1 = [E_{ads}(OH_{(a)}) + E_{ads}(H_{(a)}) - E_{ads}(H_2O_{(a)})] + [E_{gas}(H_{(g)}) + E_{gas}(OH_{(g)}) - E_{gas}(H_2O_{(g)})] + [E_{corr}(CO_{(a)} + OH_{(a)} + H_{(a)}) - E_{corr}(CO_{(a)} + H_2O_{(a)})] \quad (4)$$

The first three terms are related to the adsorption energies of products, $OH_{(a)}$ and $H_{(a)}$, and desorption energy ($-E_{ads}$) of the reactant, $H_2O_{(a)}$. The fourth to sixth terms correspond to the gas phase dissociation of $H_2O_{(g)}$. The last two terms are related to the correction energy from the adsorbate effect, while $CO_{(a)}$ coadsorbed on the surface as a spectator and can be expressed as

$$E_{corr}(CO_{(a)} + H_2O_{(a)}) = E_{ads}(CO_{(a)} + H_2O_{(a)}) - [E_{ads}(CO_{(a)}) + E_{ads}(H_2O_{(a)})] \quad (5)$$

$$E_{corr}(CO_{(a)} + OH_{(a)} + H_{(a)}) = E_{ads}(CO_{(a)} + OH_{(a)} + H_{(a)}) - [E_{ads}(CO_{(a)}) + E_{ads}(OH_{(a)}) + E_{ads}(H_{(a)})] \quad (6)$$

$E_{ads}(CO_{(a)} + H_2O_{(a)})$ and $E_{ads}(CO_{(a)} + OH_{(a)} + H_{(a)})$ are the coadsorption energies of $CO_{(a)} + H_2O_{(a)}$ and $CO_{(a)} + OH_{(a)} + H_{(a)}$ on the surface, respectively.

Similarly, the reaction energies of the other steps can be divided and expressed as

$$\Delta H_2 = [E_{ads}(cis\text{-}COOH_{(a)}) - E_{ads}(CO_{(a)}) - E_{ads}(OH_{(a)})] + [E_{gas}(COOH_{(g)}) - E_{gas}(CO_{(g)}) - E_{gas}(OH_{(g)})] + [E_{corr}(cis\text{-}COOH_{(a)} + H_{(a)}) - E_{corr}(CO_{(a)} + OH_{(a)} + H_{(a)})] \quad (7)$$

$$\Delta H_3 = [E_{ads}(CO_{2(a)}) + E_{ads}(H_{(a)}) - E_{ads}(cis\text{-}COOH_{(a)})] + [E_{gas}(CO_{2(g)}) + E_{gas}(H_{(g)}) - E_{gas}(COOH_{(g)})] + [E_{corr}(CO_{2(a)} + 2H_{(a)}) - E_{corr}(cis\text{-}COOH_{(a)} + H_{(a)})] \quad (8)$$

$$\Delta H_4 = [E_{ads}(O_{(a)}) + E_{ads}(H_{(a)}) - E_{ads}(OH_{(a)})] + [E_{gas}(H_{(g)}) + E_{gas}(O(g)) - E_{gas}(OH_{(g)})] + [E_{corr}(CO_{(a)} + O_{(a)} + 2H_{(a)}) - E_{corr}(CO_{(a)} + OH_{(a)} + H_{(a)})] \quad (9)$$

$$\Delta H_5 = [E_{ads}(CO_{(2a)}) - E_{ads}(CO_{(a)}) - E_{ads}(O_{(a)})] + [E_{gas}(CO_{2(g)}) - E_{gas}(CO_{(g)}) - E_{gas}(O_{(g)})] + [E_{corr}(CO_{2(a)} + 2H_{(a)}) - E_{corr}(CO_{(a)} + O_{(a)} + 2H_{(a)})] \quad (10)$$

$$\Delta H_6 = [E_{ads}(H_{2(g)}) - 2 \times E_{ads}(H_{(a)})] + [E_{gas}(H_{2(g)}) - 2 \times E_{gas}(H_{(g)})] + [E_{corr}(CO_{2(g)} + H_{2(g)}) - E_{corr}(CO_{2(a)} + 2H_{(a)})] \quad (11)$$

The related correction energies can be represented as

$$E_{corr}(cis\text{-}COOH_{(a)} + H_{(a)}) = E_{ads}(cis\text{-}COOH_{(a)} + H_{(a)}) - [E_{ads}(cis\text{-}COOH_{(a)}) + E_{ads}(H_{(a)})] \quad (12)$$

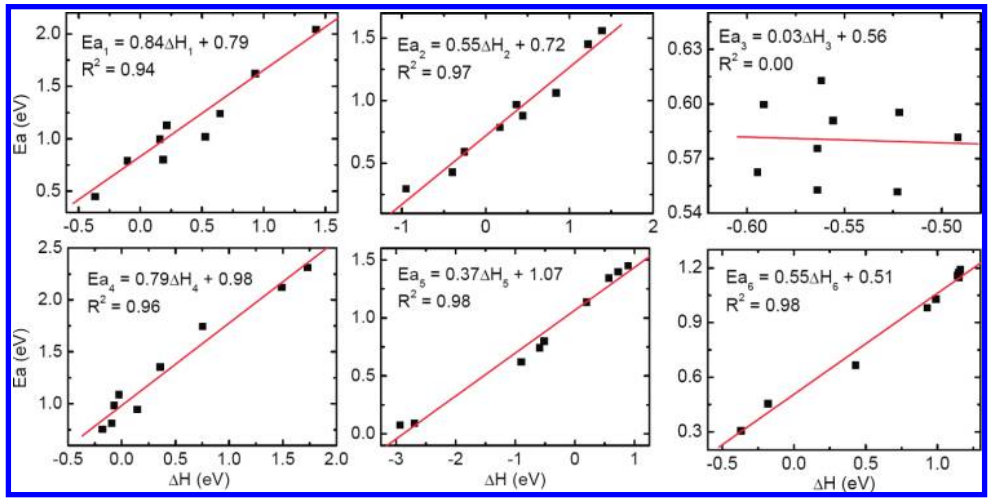

Figure 6. BEP plots of Ea against ΔH for all the elementary steps in reactions 2 and 3.

$$E_{corr}(CO_{2(a)} + 2H_{(a)}) = E_{ads}(CO_{2(a)} + 2H_{(a)}) - [E_{ads}(CO_{2(a)}) + 2 \times E_{ads}(H_{(a)})] \quad (13)$$

$$E_{corr}(CO_{(a)} + O_{(a)} + 2H_{(a)}) = E_{ads}(CO_{(a)} + O_{(a)} + 2H_{(a)}) - [E_{ads}(CO_{(a)}) + E_{ads}(O_{(a)}) + 2 \times E_{ads}(H_{(a)})] \quad (14)$$

$$E_{corr}(CO_{2(g)} + H_{2(g)}) = E_{ads}(CO_{2(g)} + H_{2(g)}) - [E_{ads}(CO_{2(g)}) + E_{ads}(H_{2(g)})] \quad (15)$$

Therefore, the reaction energies of all six elementary steps can be simply attributed to the three kinds of energies: adsorption (or desorption), gas-phase reaction, and correction energies. First, correction energies of all the elementary steps (Table S5, Supporting Information) are relatively small, <0.30 eV, and can be ignored. Second, gas-phase reaction energies are only related to the properties of the gas-phase molecules, but not to the metal surfaces. Therefore, trends of ΔH on the close-packed metal surfaces can be directly corresponded to trends of desorption and adsorption energies of reactants and products, respectively. This conclusion is similar to a previous work in the study of bond formation trends on 4d-metal surfaces.[67]

In the first O−H bond dissociation step, ΔH_1 (eq 4) is dominated by the adsorption energies of $E_{ads}(OH_{(a)})$, −3.64 to −2.21 eV, and $E_{ads}(H_{(a)})$, −2.87 to −2.09 eV, while the desorption energy of $H_2O_{(a)}$ is rather small, 0.12−0.39 eV. The stronger adsorption energies of $OH_{(a)}$ and $H_{(a)}$ on the surfaces of upper-left elements, such as Co(111), Ni(111), and Rh(111), result in the smallest ΔH_1, −0.37, −0.11, and 0.16 eV, respectively. Similarly, in the second O−H bond breaking step, the strong adsorption energy of $E_{ads}(O_{(a)})$, − 5.93 to −3.56 eV, has the major contribution to ΔH_4, as shown in eq 9. The weakest adsorption of $O_{(a)}$ on the surfaces of lower-right metals, such as Ag(111) and Au(111), results in the highest ΔH_4, 1.73 and 1.49 eV, respectively.

In the C−O bond formation step of $CO_{(a)} + OH_{(a)} + H_{(a)} \rightarrow$ *cis*-$COOH_{(a)} + H_{(a)}$, ΔH_2 (eq 7) mainly corresponds to the desorption energies of $CO_{(a)}$ ($-E_{ads}(CO_{(a)})$) and $OH_{(a)}$ ($-E_{ads}(OH_{(a)})$) since E_{ads}(*cis*-$COOH_{(a)}$) is relatively lower. The larger desorption energies of $CO_{(a)}$ and $OH_{(a)}$, related to their stronger adsorption energies, yield the high endothermicity of ΔH_2 on the surfaces of upper-left elements. Similarly, in the other C−O bond formation step of $CO_{(a)} + O_{(a)} + 2H_{(a)} \rightarrow CO_{2(a)} + 2H_{(a)}$, the higher endothermicity of ΔH_5 on Co(111), Ni(111), and Rh(111) also corresponds to their stronger $CO_{(a)}$ and $O_{(a)}$ adsorptions.

As a result, the opposite trends of reaction energies between the O−H bond dissociation (ΔH_1 and ΔH_4) and the C−O bond formation (ΔH_2 and ΔH_5) steps can be attributed to the stronger adsorption energies of products and higher desorption energies of reactants, respectively. On the other hand, weaker adsorption energies of all adspieces on the surfaces of lower-right metals (Ag, Pt, Ag) yield higher (endothermic) and lower (exothermic) ΔH in O−H bond dissociation and C−O bond formation steps, respectively. In addition, the excellent BEP relationship between ΔH and Ea (Figure 6) indicates that lower barriers in O−H bond dissociation, Ea_1 and Ea_4, will occur on the upper-left metal surfaces, while smaller barriers in C−O bond formation, Ea_2 and Ea_5, will take place on lower-right metal surfaces. Since the WGSR activity of metal/oxides is related to C−O bond formation steps, the higher activity of Cu-, Ag-, Pt-, and Au-based catalysts can be attributed to their weaker adsorption energies of $CO_{(a)}$, $OH_{(a)}$, and $O_{(a)}$.

On the basis of the analysis of adsorption energy, surfaces with stronger adsorption energies will yield lower bond-dissociation and higher bond-formation barriers. This conclusion can further be applied to other catalytic reactions. If the catalytic reaction is controlled by bond dissociation steps, such as ethanol decomposition, upper-left metal surfaces with stronger adsorption energies are expected to show better catalytic efficiency. This prediction agrees well with previous calculation[85−88] and experiments[87−90] that Ni(111) and Rh(111) have better capability to break a C−C bond and decompose ethanol efficiently. If the catalytic reaction is dominated by the bond formation step, such as CO oxidation, the higher activity on lower-right metal catalysts can be anticipated due to their weaker adsorption energies. This assumption is also consistent with computational[39,41,55−57,60,62,64] and experimental[91−96] works, which Cu, Ag, Pt, and Au are considered as the best catalysts for CO oxidation.

It is also worth noting that the insensitivity of ΔH_3 on these metal surfaces can also be justified from trends of adsorption energies. The reaction energy of ΔH_3 (eq 8) corresponds to the differences between E_{ads}(*cis*-$COOH_{(a)}$) and $E_{ads}(H_{(a)})$ since $E_{ads}(CO_{2(a)})$ is negligible (Table 1). The difference on each metal surface is rather small, and no observable trends can be found.

DOS Analysis. Trends of adsorption energies can effectively predict activities of various catalytic reactions as described above. Furthermore, the detailed chemistry of these trends can

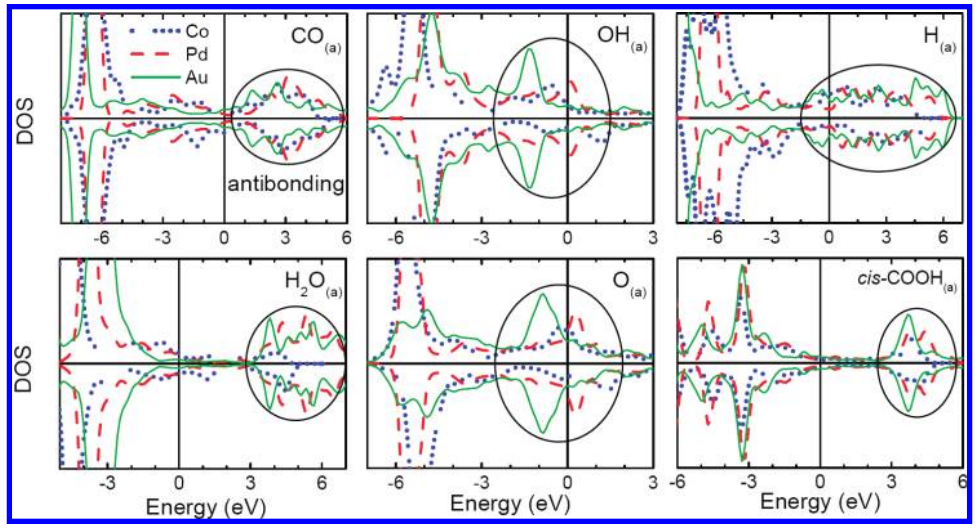

Figure 7. DOS of adsorbates for $CO_{(a)}$, $H_2O_{(a)}$, $OH_{(a)}$, $O_{(a)}$, $H_{(a)}$, and *cis*-$COOH_{(a)}$, on Co(111), Pd(111), and Au(111), are shown in blue-dot, red-dash, and green lines, respectively. The antibonding states of metal−adsorbate bonds are indicated in the circle.

be understood from the DOS analysis. The DOS of adsorbates for $CO_{(a)}$, $H_2O_{(a)}$, $OH_{(a)}$, $O_{(a)}$, $H_{(a)}$, and *cis*-$COOH_{(a)}$ on Co(111), Pd(111), and Au(111) are shown in Figure 7 for brevity. The DOS of clean and adsorbed surfaces of all selected metals are shown in the Supporting Information (Figures S1−S7).

The strength of the adsorption energy can be attributed to the antibonding state of the metal−adsorbate bond, as circled in Figure 7. The antibonding state, which will be influenced by the DOS of surfaces, with lower energy relative to the Fermi level is easier to be filled and results in a weaker adsorption, such as adsorptions on Au(111). A downward shifted antibonding state relative to the Fermi level corresponds to the downward shifted DOS of the surface. In addition, the broader DOS of the surface will further pull down the antibonding state. As a result, the DOS of a metal surface with lower energy and broader distribution, such as Au(111), will lead to a lower antibonding state and weaker adsorption, similar to the description in the d-band theory.[97−99]

In the present calculation, the DOS of the close-packed metal surfaces are only related to electronic structures of metals, and no geometrical effect is involved due to their identical crystal structure and surface orientation. In a column comparison, DOS energies of group 11 surfaces, Cu(111), Ag(111), and Au(111), are relatively deeper below the Fermi level than those of group 9 (Co, Rh, and Ir) and 10 (Ni, Pd, and Pt) surfaces. This result can be attributed to that coinage metals with fulfilled d orbitals have lower orbital energies. In the row comparison, the bottom elements of 5d surfaces, Ir(111), Pt(111), and Au(111), have relatively broader DOS distribution than 3d (Co, Ni, and Cu) and 4d (Rh, Pd, and Ag) surfaces because of the weaker interaction between the nuclear and 5d orbitals. Therefore, trends of adsorption energies (Figure 2) are essentially related to the trends of d-orbital energies, decreasing from left to right across a period, and delocalization, increasing down a group.

Charge Density. Trends of adsorption energies can also be emphasized from the charge analysis. Bader charges of each adsorbate on the close-packed metal surfaces are shown in Figure 8, and those of each atom are specified in Table S8 (Supporting Information). Metal surfaces carry the same amount of charges as adsorbates with an opposite sign since the net charge of the whole system is zero. Fewer charges on the adsorbate indicate that fewer electrons are involved in the metal−adsorbate bond and result in a weaker adsorption.

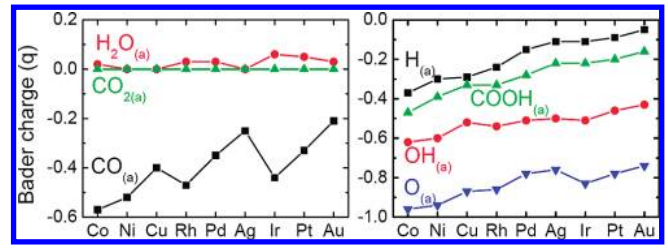

Figure 8. Bader charges of reactants, product (left), and intermediates (right) on the close-packed metal surfaces. The specific charges of each atom are listed in Table S8 (Supporting Information).

Therefore, trends of Bader charges in Figure 8 are similar to those of adsorption energies in Figure 2.

Furthermore, the variation of charge induced upon adsorption, $\Delta\rho$ = (adsorption) − ρ(surface) − ρ(adsorbate), can also be applied to understand the correlation between adsorption energies and Ea. Induced charge rearrangement of the transition states in the O−H bond dissociation (TS1 and TS4) and the C−O bond formation (TS2 and TS5) steps on Co(111) and Au(111), for example, is analyzed in Figure 9. The charge analysis of transition states on all metal surfaces is shown in the Supporting Information (Figures S8−S11).

In the O−H bond dissociation steps, TS1 and TS4 on Co(111) show higher induced charges between the surface and dissociating species than those on Au(111). The higher induced charge indicates the stronger interaction that can stabilize the fragments and lower Ea_1 and Ea_4 on Co(111). On the other hand, TS2 and TS5 on Co(111) also show higher induced charges and stronger interaction between the surface and adspecies than those on Au(111) in the C−O bond formation steps. However, the stronger interaction will hinder the desorption of adspecies ($OH_{(a)}$ and $O_{(a)}$) in the bond formation steps and raise Ea_2 and Ea_5 on Co(111). As a result, the opposite trends between two kinds of transition states in Figure 5 can be attributed to that the stronger adsorption energy (surface−adspecies interaction) will decrease and increase Ea in bond dissociation and formation steps, respectively.

Conclusion

The mechanism of WGSR has been systematically examined and compared on the close-packed metal surfaces. The WGSR activity of pure-metal catalysts is related to the Ea in both O−H

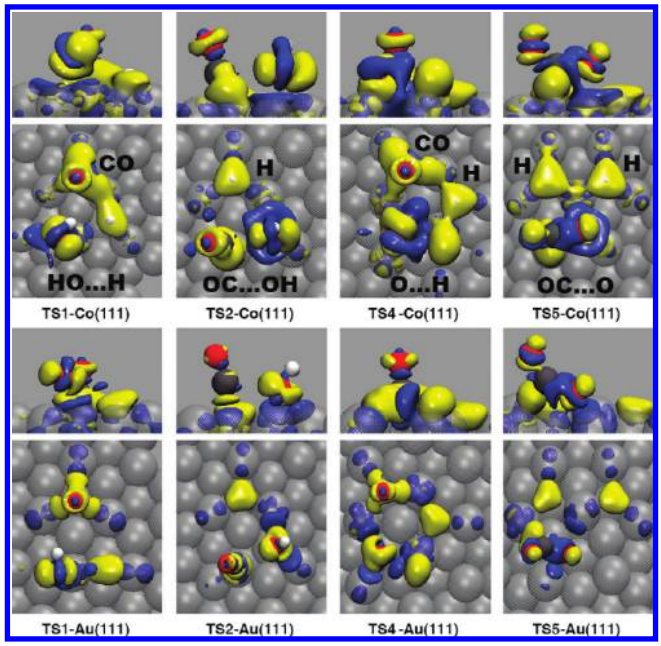

Figure 9. Induced charge rearrangement of the transitions states in O−H bond dissociation (TS1 and TS4) and C−O formation (TS2 and TS5) on Co(111) and Au(111). Blue and yellow isosurfaces indicate depletion and addition of $0.03e^{-}/Å^{3}$, respectively, referenced to the separated system. Gray, red, white and transparent silver spheres mark C, O, H, and metal atoms, respectively. Top and bottom panels for each pair of images represent side and top views.

bond dissociation and C−O bond formation steps. The activity of metal/oxide catalysts, however, depends only on the Ea in C−O bond formation steps. The computed result shows that O−H bond dissociation barriers increase as metal surfaces move from left to right and up to down across the Periodic Table. On the other hand, C−O bond formation barriers have an opposite trend. As a result, the best catalytic activity of Cu-based catalysts can be attributed to its mild barriers in both bond dissociation and formation steps. In addition, the excellent WGSR performance of (Cu, Ag, Pt, Au)/(TiO_2, CeO_2) corresponds to lower C−O bond formation barriers on the surfaces of lower-right d-block metals.

Trends of ΔH and Ea have been further analyzed in the view of adsorption energy, DOS, and charge density. In the analysis of adsorption energy, ΔH is mainly affected by adsorption and desorption energies of products and reactants, respectively. The stronger adsorption (or higher desorption energies) results in a lower and higher ΔH (or Ea) in bond dissociation and formation steps, respectively. Furthermore, the adsorption energy corresponds to the antibonding state and can be essentially related to the d-orbital energy and delocalization of metal surfaces in the DOS analysis. Trends of d-orbital energy, groups 9 > 10 > 11, and delocalization, 3d < 4d <5d, are responsible for the computed result of adsorption energies. Finally, the charge analysis of transition states further confirms the correlation between the adsorption energy and Ea that the strong surface−adsorbate interaction with higher induced charges will stabilize dissociating fragments and lower O−H bond dissociation barriers. On the other hand, these stronger adsorptions will retard adspecies desorptions and raise Ea in C−O bond formation steps.

Acknowledgment. This work is supported by the National Science Council, Taiwan (NSC 98-2113-M-003-003-MY2). CPU time from Taiwan's National Center for High-performance Computing (NCHC) and the Institute of Nuclear Energy Research (INER) is greatly appreciated.

Supporting Information Available: Extensive tables and figures. This material is available free of charge via the Internet at http://pubs.acs.org.

References and Notes

(1) Navarro, R. M.; Pena, M. A.; Fierro, J. L. G. *Chem. Rev.* **2007**, *107*, 3952.
(2) Yeung, C. M. Y.; Yu, K. M. K.; Fu, Q. J.; Thompsett, D.; Petch, M. I.; Tsang, S. C. *J. Am. Chem. Soc.* **2005**, *127*, 18010.
(3) Hardacre, C.; Ormerod, R. M.; Lambert, R. M. *J. Phys. Chem.* **1994**, *98*, 10901.
(4) Gorte, R. J.; Zhao, S. *Catal. Today* **2005**, *104*, 18.
(5) Grenoble, D. C.; Estadt, M. M.; Ollis, D. F. *J. Catal.* **1981**, *67*, 90.
(6) Hilaire, S.; Wang, X.; Luo, T.; Gorte, R. J.; Wagner, J. *Appl. Catal., A* **2001**, *215*, 271.
(7) Jacobs, G.; Chenu, E.; Patterson, P. M.; Williams, L.; Sparks, D.; Thomas, G.; Davis, B. H. *Appl. Catal., A* **2004**, *258*, 203.
(8) Jacobs, G.; Patterson, P. M.; Graham, U. M.; Sparks, D. E.; Davis, B. H. *Appl. Catal., A* **2004**, *269*, 63.
(9) Lei, Y.; Cant, N. W.; Trimm, D. L. *Catal. Lett.* **2005**, *103*, 133.
(10) Panagiotopoulou, P.; Kondarides, D. I. *J. Catal.* **2004**, *225*, 327.
(11) Panagiotopoulou, P.; Kondarides, D. I. *Catal. Today* **2006**, *112*, 49.
(12) Wang, X.; Gorte, R. J. *Appl. Catal., A* **2003**, *247*, 157.
(13) Wang, X.; Gorte, R. J.; Wagner, J. P. *J. Catal.* **2002**, *212*, 225.
(14) Wheeler, C.; Jhalani, A.; Klein, E. J.; Tummala, S.; Schmidt, L. D. *J. Catal.* **2004**, *223*, 191.
(15) Haryanto, A.; Fernando, S. D.; To, S. D. F.; Steele, P. H.; Pordesimo, L.; Adhikari, S. *Energy Fuels* **2009**, *23*, 3097.
(16) Velu, S.; Suzuki, K.; Kapoorb, M. P.; Ohashia, F.; Osaki, T. *J. Catal.* **2001**, *213*, 47.
(17) Tibiletti, D.; BartdeGraaf, E. A.; Teh, S. P.; Rothenberg, G.; Farrusseng, D.; Mirodatos, C. *J. Catal.* **2004**, *225*, 489.
(18) Park, J. B.; Graciania, J.; Evansb, J.; Stacchiolaa, D.; Maa, S.; Liua, P.; Nambua, A.; Sanzc, J. F.; Hrbek, J.; Rodrigueza, J. A. *Proc. Natl. Acad. Sci. U.S.A.* **2009**, *106*, 4975.
(19) Rim, K. T.; Eom, D.; Liu, L.; Stolyarova, E.; Raitano, J. M.; Chan, S.-W.; Flytzani-Stephanopoulos, M.; Flynn, G. W. *J. Phys. Chem. C* **2009**, *113*, 10198.
(20) Rodriguez, J. A.; Evans, J.; Graciani, J.; Park, J.-B.; Liu, P. *J. Phys. Chem. C* **2009**, *113*, 7364.
(21) Rodriguez, J. A.; Graciani, J.; Evans, J.; Park, J. B.; Yang, F.; Stacchiola, D.; Senanayake, S. D.; Ma, S.; Pérez, M.; Liu, P.; Sanz, J. F.; Hrbek, J. *Angew. Chem., Int. Ed.* **2009**, *48*, 8047.
(22) Rodriguez, J. A.; Ma, S.; Liu, P.; Hrbek, J.; Evans, J.; Pérez, M. *Science* **2007**, *318*, 1757.
(23) Yeung, C. M. Y.; Tsang, S. C. *J. Phys. Chem. C* **2009**, *113*, 6074.
(24) Park, J. B.; Graciani, J.; Evans, J.; Stacchiola, D.; Senanayake, S. D.; Barrio, L.; Liu, P.; Sanz, J. F.; Hrbek, J.; Rodriguez, J. A. *J. Am. Chem. Soc.* **2010**, *132*, 356.
(25) Estrella, M.; Barrio, L.; Zhou, G.; Wang, X.; Wang, Q.; Wen, W.; Hanson, J. C.; Frenkel, A. I.; Rodriguez, J. A. *J. Phys. Chem. C* **2009**, *113*, 14411.
(26) Fu, Q.; Saltsburg, H.; Flytzani-Stephanopoulos, M. *Science* **2003**, *301*, 935.
(27) Yeung, C. M. Y.; Meunier, F.; Burch, R.; Thompsett, D.; Tsang, S. C. *J. Phys. Chem. B* **2006**, *110*, 8540.
(28) Rodriguez, J. A.; Hanson, J. C.; Wen, W.; Wang, X.; Brito, J. L.; Martinez-Arias, A.; Fernandez-Garcia, M. *Catal. Today* **2009**, *145*, 188.
(29) Rodriguez, J. A.; Wang, X.; Liu, P.; Wen, W.; Hanson, J. C.; Hrbek, J.; Perez, M.; Evans, J. *Topics Catal.* **2007**, *44*, 73.
(30) Jacobs, G.; Williams, L.; Graham, U.; Sparks, D.; Davis, B. H. *J. Phys. Chem. B* **2003**, *107*, 10398.
(31) Jacobs, G.; Graham, U. M.; Chenu, E.; Patterson, P. M.; Dozier, A.; Davis, B. H. *J. Catal.* **2005**, *229*, 499.
(32) Rodriguez, J. A.; Liu, P.; Hrbek, J.; Evans, J.; Perez, M. *Angew. Chem., Int. Ed.* **2007**, *46*, 1329.
(33) Yen, C.-W.; Lin, M.-L.; Wang, A.; Chen, S.-A.; Chen, J.-M.; Mou, C.-Y. *J. Phys. Chem. C* **2009**, *113*, 17831.
(34) Iida, H.; Igarash, A. *Appl. Catal., A* **2006**, *303*, 48.
(35) Hornes, A.; Hungria, A. B.; Bera, P.; Camara, A. L.; Fernandez-Garcia, M.; Martinez-Arias, A.; Barrio, L.; Estrella, M.; Zhou, G.; Fonseca, J. J.; Hanson, J. C.; Rodriguez, J. A. *J. Am. Chem. Soc.* **2010**, *132*, 34.
(36) Gokhale, A. A.; Dumesic, J., A.; Mavrikakis, M. *J. Am. Chem. Soc.* **2008**, *130*, 1402.
(37) Liu_, P.; Rodriguez, J. A. *J. Chem. Phys.* **2007**, *126*, 164705.
(38) Grabow, L. C.; Gokhale, A. A.; Evans, S. T.; Dumesic, J. A.; Mavrikakis, M. *J. Phys. Chem. C* **2008**, *112*, 4608.

(39) Su, H.-Y.; Yang, M.-M.; Bao, X.-H.; Li, W.-X. *J. Phys. Chem. C* **2008**, *112*, 17303.
(40) Wang, Y.; Zhang, D.; Zhu, R.; Zhang, C.; Liu, C. *J. Phys. Chem. C* **2009**, *113*, 6215.
(41) Ojifinni, R. A.; Froemming, N. S.; Gong, J.; Pan, M.; Kim, T. S.; White, J. M.; Henkelman, G.; Mullins, C. B. *J. Am. Chem. Soc.* **2008**, *130*, 6801.
(42) Liu, Z.-P.; Jenkins, S. J.; King, D. A. *Phys. Rev. Lett.* **2005**, *94*, 196102.
(43) Kinch, R. T.; Cabrera, C. R.; Ishikawa, Y. *J. Phys. Chem. C* **2009**, *113*, 9239.
(44) Kresse, G.; Hafner, J. *Phys. Rev. B* **1993**, *47*, 558.
(45) Kresse, G.; Hafner, J. *Phys. Rev. B* **1994**, *49*, 1425.
(46) Kresse, G.; Furthmüller, J. *Phys. Rev. B* **1996**, *54*, 11169.
(47) Cleperley, D. M.; Alder, B. J. *Phys. Rev. Lett.* **1980**, *45*, 566.
(48) Perdew, J. P.; Yang, Y. *Phys. Rev. B* **1992**, *45*, 244.
(49) Blöchl, P. E. *Phys. Rev. B* **1994**, *50*, 17953.
(50) Kresse, G.; Joubert, D. *Phys. Rev. B* **1999**, *59*, 1758.
(51) Monkhorst, H. J.; Pack, J. D. *Phys. Rev. B* **1976**, *13*, 5188.
(52) Mills, G.; Jonsson, H.; Schenter, G. K. *Surf. Sci.* **1995**, *324*, 305.
(53) Breen, J. P.; Burch, R.; Coleman, H. M. *Appl. Catal., B* **2002**, *39*, 65.
(54) Chen, H.-T.; Chang, J.-G.; Ju, S.-P.; Chen, H.-L. *J. Comput. Chem.* **2010**, *31*, 258.
(55) Camellone, M. F.; Fabris, S. *J. Am. Chem. Soc.* **2009**, *131*, 10473.
(56) Chou, J.-P.; Pai, W. W.; Kuo, C.-C.; Lee, J. D.; Lin, C. H.; Wei, C.-M. *J. Phys. Chem. C* **2009**, *113*, 13151.
(57) Gong, J.; Mullins, C. B. *Acc. Chem. Res.* **2009**, *42*, 1063.
(58) Gong, J.; Mullins, C. B. *J. Am. Chem. Soc.* **2009**, *131*, 10473.
(59) Wang, F.; Zhang, D.; Xu, X.; Ding, Y. *J. Phys. Chem. C* **2009**, *113*, 18032.
(60) Wang, H.-F.; Gong, X.-Q.; Guo, Y.-L.; Guo, Y.; Lu, G.; Hu, P. *J. Phys. Chem. C* **2009**, *113*, 6124.
(61) Wang, J. G.; Hammer, B. *Phys. Rev. Lett.* **2006**, *97*, 136107.
(62) Zhang, J.; Jin, H.; Sullivan, M. B.; Lim, F. C. H.; Wu, P. *Phys. Chem. Chem. Phys.* **2009**, *11*, 1441.
(63) Gajdos, M.; Eichler, A.; Hafner, J. *J. Phys.: Condens. Matter* **2004**, *16*, 1141.
(64) Kandoi, S.; Gokhale, A. A.; Grabow, L. C.; Dumesic, J. A.; Mavrikakis, M., *Catal. Lett.* **2004**, 93.
(65) Greeley, J.; Mavrikakis, M. *J. Catal.* **2002**, *208*, 291.
(66) Neyman, K. M.; Lim, K. H.; Chen, Z.-X.; Moskaleva, L. V.; Bayer, A.; Reindl, A.; Borgmann, D.; Denecke, R.; Steinrück, H.-P.; Rösch, N. *Phys. Chem. Chem. Phys.* **2007**, *9*, 3470.
(67) Crawford, P.; Hu, P. *J. Chem. Phys.* **2007**, *126*, 194706.
(68) Ford, D. C.; Xu, Y.; Mavrikakis, M. *Surf. Sci.* **2005**, *587*, 159.
(69) Phatak, A. A.; Delgass, W. N.; Ribeiro, F. H.; Schneider, W. F. *J. Phys. Chem. C* **2009**, *113*, 7269.
(70) Michaelides, A.; Hu, P. *J. Am. Chem. Soc.* **2001**, *123*, 4235.
(71) Barton, D. G.; Podkolzin, S. G. *J. Phys. Chem. B* **2005**, *109*, 2262.
(72) Wang, G.-C.; Tao, S.-X.; Bu, X.-H. *J. Catal.* **2006**, *244*, 10.
(73) Mavrikakis, M.; Rempel, J.; Greeley, J.; Hansen, L. B.; Norskov, J. K. *J. Chem. Phys.* **2002**, *117*, 6737.
(74) Xu, Y.; Mavrikakis, M. *J. Chem. Phys.* **2002**, *116*, 10846.
(75) Eichler, A.; Mittendorfer, F.; Hafner, J. *Phys. Rev. B* **2000**, *62*, 4744.
(76) Greeley, J.; Mavrikakis, M. *Nat. Mater.* **2004**, *3*, 810.
(77) Pozzo, M.; Carlini, G.; Rosei, R. *J. Chem. Phys.* **2007**, *126*, 164706.
(78) Cao, Y.; Chen, Z.-X. *Surf. Sci.* **2006**, *600*, 4572.
(79) Crawford, P.; McAllister, B.; Hu, P. *J. Phys. Chem. C* **2009**, *113*, 5222.
(80) Michaelides, A.; Liu, Z.-P.; Zhang, C. J.; Alavi, A.; King, D. A.; Hu, P. *J. Am. Chem. Soc.* **2003**, *125*, 3704.
(81) Gong, X.-Q.; Liu, Z.-P.; Raval, R.; Hu, P. *J. Am. Chem. Soc.* **2004**, *126*, 8.
(82) Nakamura, J.; Campbell, J. M.; Campbell, C. T. *J. Chem. Soc., Faraday Trans.* **1990**, *86*, 2725.
(83) Fronzi, M.; Piccinin, S.; Delley, B.; Traversa, E.; Stampfl, C. *Phys. Chem. Chem. Phys.* **2009**, *11*, 9188.
(84) Zhang, C.; Lindan, P. J. D. *J. Chem. Phys.* **2004**, *121*, 3811.
(85) Wang, J.-H.; Lee, C. S.; Lin, M. C. *J. Phys. Chem. C* **2009**, *113*, 6681.
(86) Yang, M.-M.; Bao, X.-H.; Li, W.-X. *J. Phys. Chem. C* **2007**, *111*, 7403.
(87) Haryanto, A.; Fernando, S.; Murali, N.; Adhikari, S. *Energy Fuels* **2005**, *19*, 2098.
(88) Ni, M.; Leung, D. Y. C.; Leung, M. K. H. *Int. J. Hydrogen Energy* **2007**, *32*, 3238.
(89) Xu, J. Z.; Zhang, X. P.; Zenobi, R.; Yoshinobu, J.; Z., X.; Yates, J. T., Jr. *Surf. Sci.* **1991**, *256*, 288.
(90) Vesseli, E.; Baraldi, A.; Comelli, G.; Lizzit, S.; Rosei, R. *ChemPhysChem* **2004**, *5*, 1133.
(91) Gao, F.; Cai, Y.; Gath, K. K.; Wang, Y.; Chen, M. S.; Guo, Q. L.; Goodman, D. W. *J. Phys. Chem. C* **2009**, *113*, 182.
(92) Gao, F.; Wang, Y.; Goodman, D. W. *J. Am. Chem. Soc.* **2009**, *131*, 5734.
(93) Gmez-Corts, A.; Daz, G.; Zanella, R.; Ramrez, H.; Santiago, P.; Saniger, J. M. *J. Phys. Chem. C* **2009**, *113*, 9710.
(94) Rodrguez-Gonzlez, V.; Zanella, R.; Calzada, L. A.; Gmez, R. *J. Phys. Chem. C* **2009**, *113*, 8911.
(95) Tanaka, K.-i.; Shou, M.; He, H.; Shi, X.; Zhang, X. *J. Phys. Chem. C* **2009**, *113*, 12427.
(96) Wu, Z.; Zhou, S.; Zhu, H.; Da, S.; Overbury, S. H. *J. Phys. Chem. C* **2009**, *113*, 3726.
(97) Hammer, B.; Norskov, J. K. *Adv. Catal.* **2000**, *45*, 71.
(98) Norskov, J. K.; Bligaard, T.; Hvolbak, B.; Abild-Pedersen, F.; Chorkendorff, I.; Christensen, C. H. *Chem. Soc. Rev.* **2008**, *37*, 2163.
(99) Stamenkovic, V.; Mun, B. S.; Mayrhofer, K. J. J.; Ross, P. N.; Markovic, N. M.; Rossmeisl, J.; Greeley, J.; Norskov, J. K. *Angew. Chem., Int. Ed.* **2006**, *45*, 2897.

JP1005814